

# Joint Estimation of Water/Fat Images and Field Inhomogeneity Map

D. Hernando,<sup>1,2\*</sup> J. P. Haldar,<sup>1,2</sup> B. P. Sutton,<sup>2,3</sup> J. Ma,<sup>4</sup> P. Kellman,<sup>5</sup> and Z.-P. Liang<sup>1,2</sup>

**Water/fat separation in the presence of  $B_0$  field inhomogeneity is a problem of considerable practical importance in MRI. This article describes two complementary methods for estimating the water/fat images and the field inhomogeneity map from Dixon-type acquisitions. One is based on variable projection (VARPRO) and the other on linear prediction (LP). The VARPRO method is very robust and can be used in low signal-to-noise ratio conditions because of its ability to achieve the maximum-likelihood solution. The LP method is computationally more efficient, and is shown to perform well under moderate levels of noise and field inhomogeneity. These methods have been extended to handle multicoil acquisitions by jointly solving the estimation problem for all the coils. Both methods are analyzed and compared and results from several experiments are included to demonstrate their performance. Magn Reson Med 59:571–580, 2008. © 2008 Wiley-Liss, Inc.**

**Key words:** dixon imaging; linear prediction; variable projection; field map estimation; IDEAL

## INTRODUCTION

Methods for separating the water and fat components in MR imaging based on their different resonance frequencies have been under intensive investigation for a number of years. Dixon's original method for water/fat separation (1) acquires two images with different echo time shifts, and models the signal in a given voxel as:

$$s(t_n) = \rho_W + e^{i2\pi f_F t_n} \rho_F \quad [1]$$

where  $t_n$  is the echo time shift. The water component has intensity  $\rho_W$  and is assumed to be exactly on resonance, while the fat component has intensity  $\rho_F$  with a known frequency shift  $f_F$  (in Hz). If the echo time shifts are chosen such that  $2\pi f_F t_n = \{0, \pi\}$ , then the two images thus

obtained will have the water and fat signals in phase and in opposed phase, respectively, and can be combined to obtain the individual water and fat components. The main limitation of this simple method arises from the presence of  $B_0$  field inhomogeneity, which introduces additional phase shifts that prevent Dixon's method from correctly separating the water and fat signals. A more realistic signal model is

$$s(t_n) = \rho_W e^{i2\pi f_B t_n} + \rho_F e^{i2\pi (f_B + f_F) t_n} \quad [2]$$

where  $f_B$  is the local frequency offset due to field inhomogeneity. In Ref. (2), a three-point method is introduced to allow estimation of  $f_B$  at each voxel. In this method, the relative phase shifts ( $2\pi f_F t_n$ ) of the water and fat signals are typically set to  $\{-\pi, 0, \pi\}$  or  $\{0, \pi, 2\pi\}$ . These choices simplify the estimation of the nonlinear parameter  $f_B$  (2).

In recent years, there has been considerable interest in alternative choices of echo shifts for three-point Dixon imaging. For arbitrary echo shifts, determination of the field inhomogeneity at each voxel cannot be decoupled from the estimation of the water/fat contributions, and the nonlinearity of the maximum-likelihood (ML) estimation problem cannot be avoided. In Refs. (3,4), a method to solve the nonlinear fitting problem, termed iterative decomposition with echo asymmetry and least-squares (IDEAL), is proposed. IDEAL consists of repeated linearizations of the original nonlinear problem, alternatively estimating the water/fat signals and the field map. Initially, this algorithm was proposed for use with fast acquisition schemes (e.g., SSFP or FSE) which constrain echo time increments to relatively small values (3,5). An analysis of the performance of water/fat decomposition under Gaussian noise is provided in Ref. (6), with the conclusion that, for three-point acquisitions, the optimal phase shifts are  $\{-\pi/6 + \pi k, \pi/2 + \pi k, 7\pi/6 + \pi k\}$ , where  $k$  is an integer.

However, the use of arbitrary phase shifts yields a nonlinear, nonconvex optimization problem for estimating the water/fat contributions and the field map. Specifically, the ML cost function will generally contain multiple local optima, and therefore iterative, descent-based algorithms cannot guarantee convergence to the global minimum. This article addresses the water/fat estimation problem with two complementary methods, which are extended to impose field map smoothness constraints and to handle multicoil acquisitions. These methods are described and analyzed in the subsequent sections.

## METHODS

Under the assumption of white additive Gaussian noise, the ML estimate estimate for  $\{\rho_W, \rho_F, f_B\}$  is obtained by

<sup>1</sup>Department of Electrical and Computer Engineering, University of Illinois at Urbana-Champaign, Urbana, Illinois

<sup>2</sup>Beckman Institute for Advanced Science and Technology, University of Illinois at Urbana-Champaign, Urbana, Illinois

<sup>3</sup>Department of Bioengineering, University of Illinois at Urbana-Champaign, Urbana, Illinois

<sup>4</sup>Department of Imaging Physics, University of Texas M. D. Anderson Cancer Center, Houston, Texas

<sup>5</sup>Laboratory of Cardiac Energetics, National Heart, Lung and Blood Institute, National Institutes of Health, Department of Health and Human Services, Bethesda, Maryland

Contract grant sponsor: NIH; Grant numbers: P41-EB03631-16, R01-CA098717

\*Correspondence to: Diego Hernando, Beckman Institute for Advanced Science and Technology, 405 N. Mathews Ave, Urbana, IL 61801. E-mail: dhernan2@uiuc.edu

Received 22 June 2007; revised 27 November 2007; accepted 28 November 2007.

DOI 10.1002/mrm.21522

Published online in Wiley InterScience (www.interscience.wiley.com).

© 2008 Wiley-Liss, Inc.

minimizing the following cost function:

$$R_0(\rho_W, \rho_F, f_B) = \sum_{n=1}^N |s(t_n) - e^{i2\pi f_B t_n}(\rho_W + \rho_F e^{i2\pi f_F t_n})|^2 \quad [3]$$

where  $N$  is the number of acquisitions with different echo times (typically  $N = 3$ ). Note that the water-fat frequency shift  $f_F$  is assumed known a priori.

This formulation corresponds to a nonlinear least squares (NLLS) optimization problem, which does not generally have a closed-form solution. In this section, we introduce two complementary algorithms to solve this problem: (a) a variable projection (VARPRO) algorithm that finds the globally optimal solution with moderate computational requirements, and (b) a computationally efficient linear prediction (LP) algorithm.

### Global Optimization Using Variable Projection

Estimation of  $\{\rho_W, \rho_F, f_B\}$  by minimizing the cost function in Eq. [3] is a separable NLLS problem. Specifically, rewrite Eq. [3] as

$$R_0(\rho, f_B) = \|\mathbf{s} - \Psi(f_B)\boldsymbol{\rho}\|_2^2 \quad [4]$$

where  $\boldsymbol{\rho} = [\rho_W \ \rho_F]^T$ ,  $\mathbf{s} = [s(t_1) \cdots s(t_N)]^T$ , and

$$\Psi(f_B) = \begin{pmatrix} e^{i2\pi f_B t_1} & e^{i2\pi(f_F+f_B)t_1} \\ e^{i2\pi f_B t_2} & e^{i2\pi(f_F+f_B)t_2} \\ \vdots & \vdots \\ e^{i2\pi f_B t_N} & e^{i2\pi(f_F+f_B)t_N} \end{pmatrix}. \quad [5]$$

For a given value of  $f_B$ , the least squares (LS) solution for the linear parameters  $\boldsymbol{\rho}$  is given by  $\Psi^\dagger(f_B)\mathbf{s}$ , where  $^\dagger$  denotes pseudoinverse. Therefore, we can remove  $\boldsymbol{\rho}$  from Eq. [4]:

$$R(f_B) = \|\mathbf{s} - \Psi(f_B)\Psi^\dagger(f_B)\mathbf{s}\|_2^2 = \|\mathbf{I} - \Psi(f_B)\Psi^\dagger(f_B)\|_2^2 \quad [6]$$

where  $\mathbf{I}$  is the  $N \times N$  identity matrix. This is the so-called VARPRO formulation of the original NLLS problem in Eq. [4]. It has been shown that  $R_0(\rho, f_B)$  and  $R(f_B)$  have the same global minimum (7,8). Using Eq. [6], the optimal linear and nonlinear parameters in Eq. [4] can be determined separately as follows

$$f_B^0 = \arg \min_{f_B} R(f_B) \quad [7]$$

$$\boldsymbol{\rho}^0 = \Psi^\dagger(f_B^0)\mathbf{s}. \quad [8]$$

This formulation has several desirable features:

- Minimization of  $R(f_B)$  in Eq. [7] is a nonconvex problem (with multiple local optima), but it is only a one-dimensional problem, which can be effectively solved using a search method. Specifically, assuming suitable bounds  $f_{B,\text{MIN}}$  and  $f_{B,\text{MAX}}$  on the field inhomogeneity, we can evaluate  $R(f_B)$  on a set of  $L$  closely spaced points  $\{f_{B,l}\}_{l=1}^L$  on the interval  $[f_{B,\text{MIN}}, f_{B,\text{MAX}}]$  and select the minimum. Thus, the presence of multiple local minima in  $R(f_B)$  does not hinder attaining the global minimizer  $f_B^0$ .
- Once  $f_B^0$  is known, estimation of  $\boldsymbol{\rho}^0$  from Eq. [8] reduces to a small matrix multiplication.

- Computation of  $\Psi^\dagger(f_B)$  for the values  $\{f_{B,l}\}_{l=1}^L$  can be performed efficiently by rewriting  $\Psi(f_B) = \Lambda(f_B)\Phi$ , where

$$\Phi = \begin{pmatrix} 1 & e^{i2\pi f_F t_1} \\ 1 & e^{i2\pi f_F t_2} \\ \vdots & \vdots \\ 1 & e^{i2\pi f_F t_N} \end{pmatrix}, \quad \text{and}$$

$$\Lambda(f_B) = \begin{pmatrix} e^{i2\pi f_B t_1} & 0 & \cdots & 0 \\ 0 & e^{i2\pi f_B t_2} & \cdots & 0 \\ \vdots & \vdots & \ddots & \vdots \\ 0 & 0 & \cdots & e^{i2\pi f_B t_N} \end{pmatrix}. \quad [9]$$

Therefore, the desired pseudoinverse is simply  $\Psi^\dagger(f_B) = \Phi^\dagger \Lambda(-f_B)$ , noting that  $\Lambda(f_B)$  is a unitary matrix and also  $\Lambda^{-1}(f_B) = \Lambda(-f_B)$ . Furthermore, only one pseudoinverse needs to be computed for the entire decomposition, even if  $\boldsymbol{\rho}$  is estimated for many different values of  $f_B$  at each voxel, since  $\Phi$  does not depend on  $f_B$  or  $\mathbf{s}$ . If  $\Phi$  has full column rank, this pseudoinverse computation reduces to  $\Phi^\dagger = [\Phi^H \Phi]^{-1} \Phi^H$ .

This application of VARPRO is similar to a recently proposed method for estimation of the  $T_1$  relaxation constant (9). Note that this formulation is flexible on the choice of the echo time shifts, although obviously at least  $N = 3$  acquisitions are required for the estimation problem to be well-posed in voxels containing both water and fat.

### Imposing Spatial Constraints

Voxel-by-voxel ML estimates may lead to erroneous decompositions at some voxels due to the presence of noise and the inherent ambiguity of the model (Eq. [2]) when a single component is present (10). To improve the water/fat separation, spatial smoothness is commonly imposed as prior knowledge on the estimate of the field map (3,11–13). Clearly, field map smoothing can be performed in a separate step, similarly to the original IDEAL algorithm (3). However, as noted in (10), this approach can be problematic if the field inhomogeneity is large (e.g.,  $f_B \geq f_F$ ) because phase shifts due to field inhomogeneity become indistinguishable from those due to the presence of different chemical species. A region-growing method is proposed in (10) to address this problem.

Within the VARPRO formulation, decoupling the estimation of  $f_B$  and  $\boldsymbol{\rho}$  allows us to effectively impose smoothness constraints on the field map. Here, we propose to use a Markov random field (MRF) prior on the field map (14). The MRF prior can be imposed efficiently using the well-known iterated conditional modes (ICM) algorithm (15). Let us denote  $\mathbf{f}_B = \{f_B^q\}_{q=1}^Q$  as the complete field map for all  $Q$  voxels. ICM iterates several times through all the voxels, updating one at a time. In this paper, we have considered simple Gaussian smoothness priors, resulting in the following update for voxel  $q$  (with neighborhood  $\delta_q$ ):

$$f_B^{q,\text{new}} = \arg \min_{f_B^q} R(f_B^q) + \mu \sum_{j \in \delta_q} w_{q,j} |f_B^q - f_B^{j,\text{cur}}|^2 \quad [10]$$

where  $f_B^{j,\text{cur}}$  is the current field inhomogeneity estimate at neighboring voxel  $j$ ,  $w_{q,j}$  are weights that control the

field difference between voxels  $q$  and  $j$ , and  $\mu$  controls the amount of smoothness imposed by the MRF. Note that, from a regularization standpoint, squared differences in the field map are penalized to enforce smoothness. Also, the results will be generally less sensitive to the choice of a few seed voxels than a region-growing method, since the complete field map estimate will be recomputed iteratively.

VARPRO requires setting several parameters. The field inhomogeneity bounds were set to almost the chemical shift between water and fat, i.e.  $\pm 200$  Hz for 1.5 T acquisitions and  $\pm 400$  Hz for 3 T acquisitions. These bounds were sufficient for all the cases presented in this article. The number of discretized field values used in the optimization was  $L = 300$ , which provides a good tradeoff between estimation accuracy and computational efficiency (see Appendix for mathematical details on the selection of the discretization step size). The MRF neighborhood employed was the square of size  $5 \times 5$  voxels centered at each voxel (excluding the center). The weights  $w_{q,j}$  were set to the inverse of the distance between voxels  $q$  and  $j$ . Finally, the regularization parameter  $\mu$  was set to  $\sigma^2/30$ , where  $\sigma^2$  is the estimated noise variance. The value of  $\sigma^2$  can be estimated from the data itself, or alternatively from prescan noise only data (16). According to the MRF model, the value of  $\mu$  is the ratio between the noise variance in the acquired images and a measure of the variability of the field map. Even though these values can be further optimized for each particular acquisition, we chose to maintain them constant throughout the results presented in this paper to highlight the robustness of the proposed method.

The VARPRO-based method with MRF prior is summarized below:

1. Initialize the field map estimate  $f_B$  (e.g., all zeros).
2. Precompute the cost function  $\{R(f_{B,l})\}_{l=1}^L$  (Eq. [6]) for a set of field inhomogeneity values  $f_{B,l} \in [f_{B,\text{MIN}}, f_{B,\text{MAX}}]$ , for all voxels.
3. For each voxel, update the field map estimate using Eq. [10].
4. Repeat step (3) until the overall field map change falls below some small threshold  $\varepsilon > 0$ :

$$\sum_{q=1}^Q |f_B^{q,\text{new}} - f_B^{q,\text{cur}}| < \varepsilon. \quad [11]$$

5. For each voxel, estimate  $\rho_W$  and  $\rho_F$  given the estimated field map using Eq. [8].

### Multicoil Acquisitions

Following (3), let us consider a multicoil acquisition with  $P$  distinct coils, which produce  $P$  images with independent amplitude weightings and phase offsets. Thus, the signal at a given voxel corresponding to coil  $p$  with echo time  $t_n$  can be modelled as

$$s_p(t_n) = e^{i2\pi f_B t_n} (\rho_{W,p} + \rho_{F,p} e^{i2\pi f_F t_n}) \quad [12]$$

where  $\rho_{W,p}$  and  $\rho_{F,p}$  are the the water and fat signal intensities, weighted by the complex-valued sensitivity of coil  $p$  at the location of the voxel under consideration.

The proposed VARPRO formulation can be extended to optimally (in the ML sense) estimate the field map as well

as the  $P$  sensitivity-weighted water/fat images. According to the signal model in Eq. [12], the new cost function is

$$R_{MC,0}(\rho_1, \dots, \rho_P, f_B) = R_{1,0}(\rho_1, f_B) + \dots + R_{P,0}(\rho_P, f_B) \quad [13]$$

where  $\rho_p = [\rho_{W,p} \ \rho_{F,p}]^T$  and  $R_{p,0}(\rho_p, f_B)$  is the single-coil cost function for the signal  $s_p$ , as defined in Eq. [4]. Clearly,  $f_B$  is the only nonlinear parameter under consideration and thus the VARPRO approach discussed earlier can be naturally extended by simply minimizing the sum of the individual cost functions. Since for each value of  $f_B$  all the linear parameters  $\{\rho_1, \dots, \rho_P\}$  are obtained immediately by solution of  $P$  linear LS problems, we can express the combined cost function in the VARPRO formulation  $R_{MC}(f_B)$  (similarly to Eq. [6]), and again a global one-dimensional search is possible to find the optimal  $f_B$  estimate.

As in the single-coil case, the water/fat amplitudes can be determined efficiently once  $f_B$  is estimated, by solving the corresponding linear problem (Eq. [8]) for each coil. After the  $P$  sensitivity-weighted water/fat images are obtained, they can be combined using standard multicoil combination techniques (3,17–19).

Here, the coil sensitivities are assumed unknown. If they are known, the VARPRO formulation can still be used, with the difference that only two component amplitudes,  $\rho_W$  and  $\rho_F$ , and the field inhomogeneity,  $f_B$ , need to be estimated at each voxel.

### Efficient Solution Using Linear Prediction

If the images are acquired at uniformly spaced echo times, a computationally faster solution is possible. Assuming the echo times are  $t_n = t_0 + n\Delta t$ ,  $n = 1, \dots, N$ , the signal model in Eq. [2] can be rewritten as follows:

$$s(t_n) = \sum_{m=1}^2 a_m z_m^n, \quad n = 1, \dots, N \quad [14]$$

where  $a_1 = \rho_W e^{i2\pi f_B t_0}$ ,  $a_2 = \rho_F e^{i2\pi (f_F + f_B) t_0}$ ,  $z_1 = e^{i2\pi f_B \Delta t}$ , and  $z_2 = e^{i2\pi (f_F + f_B) \Delta t}$ .

This signal, in the absence of noise, is linearly predictable with coefficients  $\{g_1, g_2\}$ , i.e.

$$s(t_n) = g_1 s(t_{n-1}) + g_2 s(t_{n-2}), \quad n = 3, \dots, N \quad [15]$$

and, since  $|z_1| = |z_2| = 1$  it is also backward-predictable with the same prediction coefficients:

$$s^*(t_n) = g_1 s^*(t_{n+1}) + g_2 s^*(t_{n+2}), \quad n = 1, \dots, N-2. \quad [16]$$

Furthermore, it can be shown that the polynomial

$$G(z) = 1 - g_1 z^{-1} - g_2 z^{-2} \quad [17]$$

has its roots at  $z_1$  and  $z_2$  (see, e.g., (20) for details).

This formulation enables an efficient determination of the parameters in the signal model (Eq. [2]). Similarly to the VARPRO method described earlier, the problem is solved by estimating the linear and nonlinear parameters in two separate steps. First, the prediction coefficients  $\{g_1, g_2\}$  are estimated using the so-called forward-backward LP by simultaneously solving Eqs. [15] and [16] (21). Next, the estimates for  $z_m$  are computed as the roots of  $G(z)$ ,

and the linear parameters  $a_m$  are obtained by solving the corresponding linear problem (Eq. [14]).

In the absence of noise, the parameters  $\{\rho_W, \rho_F, f_B\}$  are obtained directly from the LP estimates  $\{a_m, z_m\}$ , as long as  $a_1 \neq 0$  and  $a_2 \neq 0$ . Denoting  $\phi_m = \angle z_m / (2\pi \Delta t)$ , then either  $\phi_2 = \phi_1 + f_F$  or  $\phi_2 = \phi_1 - f_F$ . Without loss of generality, we can sort  $\{\phi_m\}$  so that the former is satisfied. Thus, the signal parameters are obtained as follows:  $f_B = \phi_1$ ,  $\rho_W = a_1 e^{-i2\pi f_B t_0}$ , and  $\rho_F = a_2 e^{-i2\pi (f_B + f_F) t_0}$ .

If one of the components is absent, the signal model becomes ambiguous (10) and assigning the observed component to water or fat requires some prior knowledge. Similarly, in the presence of noise, the frequency separation of the observed components will not be exactly  $f_F$ . Assuming a limited range on the field inhomogeneity,  $[f_{B,\text{MIN}}, f_{B,\text{MAX}}]$ , we propose to assign to water and fat the component with estimated frequency  $\phi_m$  closest to 0 and  $f_F$ , respectively, i.e., the component minimizing

$$\phi_W = \arg \min_{\phi \in \{\phi_1, \phi_2\}} |\phi|, s.t. \phi \in [f_{B,\text{MIN}}, f_{B,\text{MAX}}] \quad [18]$$

is assigned to water (with corresponding amplitude  $\rho_W = a_W e^{-i2\pi f_B t_0}$ ), and the component minimizing

$$\phi_F = \arg \min_{\phi \in \{\phi_1, \phi_2\}} |\phi - f_F|, s.t. \phi \in [f_F + f_{B,\text{MIN}}, f_F + f_{B,\text{MAX}}] \quad [19]$$

is assigned to fat (with amplitude  $\rho_F = a_F e^{-i2\pi (f_B + f_F) t_0}$ ).

If no estimated frequency  $\phi_m$  lies within the specified bounds for a given component, this component is assumed not present at the current voxel. Subsequently, the field map value can be estimated at each voxel by weighted averaging of the individual estimated field inhomogeneities:

$$f_{B,v} = \frac{\phi_W |\rho_W| + (\phi_F - f_F) |\rho_F|}{|\rho_W| + |\rho_F|}. \quad [20]$$

### Imposing Spatial Constraints

The voxel-by-voxel LP-based method typically produces rougher field map estimates than VARPRO, due to the suboptimal nature of LP for solving the NLLS fitting problem (minimizing Eq. [3]) in the presence of noise. Thus, the LP field map estimate can benefit from spatial regularization. However, the LP formulation does not provide the same flexibility as VARPRO for incorporating spatial constraints. Here, we propose to impose smoothness on the field map in a separate step, by penalizing deviations from the voxel-by-voxel estimates as well as field map roughness. This can be formulated effectively as a regularized LS problem:

$$\hat{f}_B = \arg \min_{f_B} [\|W(f_B - f_{B,v})\|^2 + \lambda \|Df_B\|^2] \quad [21]$$

where  $f_B$  is the complete field map (a length- $Q$  vector corresponding to the  $Q$  voxels in the image),  $f_{B,v}$  is the rough field map estimated independently at each voxel (Eq. [20]),  $W$  is a diagonal weighting matrix used to place more weight on field map estimates from voxels where the signal level is higher,  $D$  computes spatial finite differences in the field map, and  $\lambda$  is a regularization parameter controlling the tradeoff between field map smoothness and data fidelity.

This minimization reduces to a linear problem:

$$(W^H W + \lambda D^H D) \hat{f}_B = W^H W f_{B,v} \quad [22]$$

and can be solved efficiently using, e.g., a conjugate-gradient method (22). This method is similar to the one proposed in (3), where the water/fat images and field map are estimated point by point and field map smoothing is performed separately. Decoupling both steps simplifies the algorithm and reduces the computational burden. It must be noted that this ‘‘two-step’’ method is suboptimal, and is expected to perform well only in cases of moderate field inhomogeneity. Specifically, the smoothing step will generally not be able to correct large errors in the field map estimate, e.g., in voxels where water and fat are swapped during voxel-by-voxel processing (10,13). Finally, the water and fat components should be reestimated at each voxel using the regularized field map  $\hat{f}_B$  by solving the corresponding linear problem (Eq. [8]).

In this article, we have employed the following parameters for LP: the weighting matrix  $W$  was set to the sum of the signal amplitudes at each voxel, normalized to have a maximum value of 1 (thus assigning more weight to the field map estimates from voxels containing higher signal amplitude). The regularization parameter  $\lambda$  was set to 1. Similarly to VARPRO, the parameters for LP were fixed throughout the results.

Since the proposed regularization of the field map will place very little weight on estimates from voxels that contain only noise (e.g., voxels where the signal amplitude is below a noise threshold), these voxels may be skipped (and their field inhomogeneity set to zero) during the voxel-by-voxel estimation, for increased computational efficiency.

The LP-based algorithm for regularized estimation of water/fat images and field map can be summarized as follows:

1. At each voxel with signal amplitude above a noise threshold, perform forward-backward LP to obtain  $z_k$  and  $a_k$  following Eqs. [15], [16], and [14]. Assign the estimated components to water/fat using Eqs. [18] and [19].
2. Obtain the regularized field map  $\hat{f}_B$  by imposing spatial smoothness (Eq. [21]).
3. Reestimate the water/fat components  $\rho_W$  and  $\rho_F$  at each voxel using the regularized field map (Eq. [8]).

### Multicoil Acquisitions

The single coil LP algorithm can easily be extended to handle multicoil acquisitions. According to the multicoil signal model in Eq. [12], the field inhomogeneity effect is the same for all coils, and furthermore the signals detected at a particular voxel by the different coils are different linear combinations of the same complex exponentials. Thus, the prediction coefficient vector is the same for all coils, which can simply be enforced by solving Eqs. [15] and [16] simultaneously for all coils. Once the prediction coefficients (and thus the  $z_k$ ) are obtained, the amplitudes of the different chemical species can be estimated independently for each coil using Eq. [14].

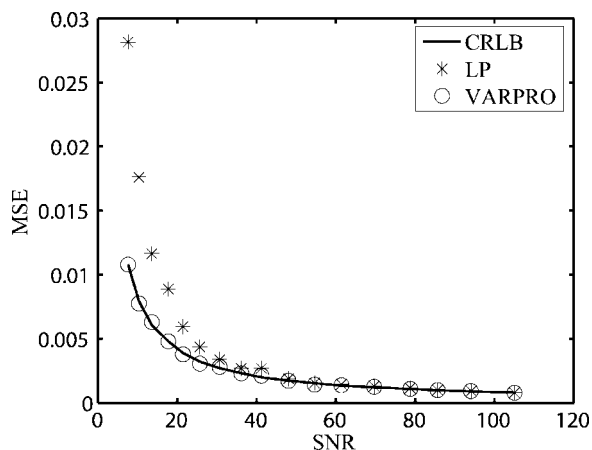


FIG. 1. Comparison between theoretical bounds (CRLB) and empirical MSE for amplitude estimation. The solid line indicates the CRLB, while the circles and asterisks represent the empirical results obtained from VARPRO and LP, respectively.

## RESULTS AND DISCUSSION

A simulation study was done to test the performance of the proposed methods for single-voxel decomposition in the presence of noise. Figure 1 shows a comparison of the Cramér-Rao lower bound (CRLB, a lower bound on the variance of any unbiased estimator (6,23)) and mean squared error (MSE) simulation results for amplitude estimation using three samples ( $N = 3$ ) with phase shifts  $\{-\pi/6, \pi/2, 7\pi/6\}$ . This choice of phase shifts is optimal for all water/fat ratios, as shown in (6). The simulated signal contains two components with amplitudes  $\rho_W = \rho_F = 1$ . Complex Gaussian noise with a range of different variances was added to the signal. The VARPRO estimate appears to be efficient (i.e., unbiased and with MSE matching the CRLB) for all SNR values. The LP estimate becomes more robust as the SNR increases. Figure 1 shows that, at lower SNR, the VARPRO approach is preferable. On the other hand, at higher SNR, LP provides a competitive and computationally efficient solution to the water/fat imaging problem.

A quantitative comparison of the accuracy of the proposed methods and IDEAL (including spatial regularization of the field map) was performed using synthetic data. Three synthetic datasets were generated, based on brain, abdominal, and cardiac acquisitions, respectively. The water and fat images were obtained by wavelet denoising the estimated water/fat components (obtained using VARPRO with no spatial regularization on the field map) from each in vivo dataset. The synthetic field maps were obtained by smoothing the corresponding voxel-by-voxel estimated field maps. This was done by applying a Hamming window in the Fourier domain. Note that the field map smoothing step in our implementation of the IDEAL algorithm was performed with the same Hamming window used to generate the synthetic field maps (3). Several field maps, simulating increasing severity of field inhomogeneity, were obtained in each case by scaling each synthetic field map. The water/fat images were then combined with each field map according to the signal model in Eq. [2] to

obtain datasets with increasing levels of field inhomogeneity. The water/fat chemical shift was 215 Hz and the the TEs produced water/fat phases  $\{-\pi/6, \pi/2, 7\pi/6\}$ . Finally, complex Gaussian noise was added to each of the datasets (SNR = 20). The noisy datasets were then processed using IDEAL, VARPRO and LP, and the resulting decompositions compared to the true images. Figure 2 shows the relative norm of the error (averaged for the brain, abdominal, and cardiac simulated datasets) in the resulting water image produced by IDEAL, VARPRO, and LP. Note how VARPRO performs almost uniformly well for all levels of field inhomogeneity, whereas the errors of LP and IDEAL increase sharply as the maximum field inhomogeneity becomes larger than  $|f_F|/2$ . This is due to the misclassifications that occur in the voxel-by-voxel decomposition, which are only partially removed in the field map smoothing step. Also, for low field inhomogeneities, LP performs nearly as well as VARPRO and IDEAL.

To test the proposed methods on in vivo data, several brain images were obtained using optimal echo spacings (4), with TE values  $\{3.38, 4.17, 4.97\}$  ms, corresponding to water/fat phases  $\{7\pi/6, \pi/2, -\pi/6\}$ . Data were acquired on a 3 T Siemens Allegra head scanner in accordance with the local institutional review board. Figure 3 shows the water/fat decomposition and field map obtained with IDEAL (3) and the proposed VARPRO and LP methods, respectively. The water/fat decompositions using all three methods are very similar. The differences observed in the estimated field map are due to the different strategies for imposing field map smoothness: (a) IDEAL filters the raw field map with a smoothing kernel (3), and thus the estimates from voxels where the signal is mostly noise are preserved; (b) VARPRO imposes a smoothing MRF prior on the field map (Eq. [10]), automatically assigning more weight to field inhomogeneity estimates from voxels with higher signal intensity; (c) LP applies a weighted LS smoothing (Eq. [21]) which has a similar effect to the MRF-based approach, since the weights applied on the field

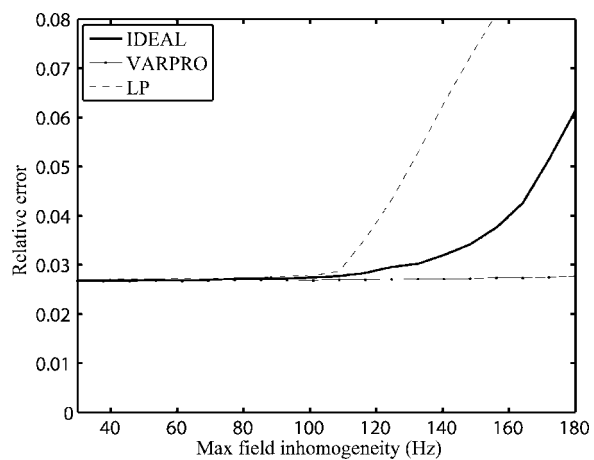


FIG. 2. Quantitative comparison of IDEAL, VARPRO, and LP for water/fat decomposition including spatial smoothness constraints on the field map. Relative errors are shown for water image reconstruction using the three methods, for different levels of field inhomogeneity, and averaged for three different synthetic datasets.

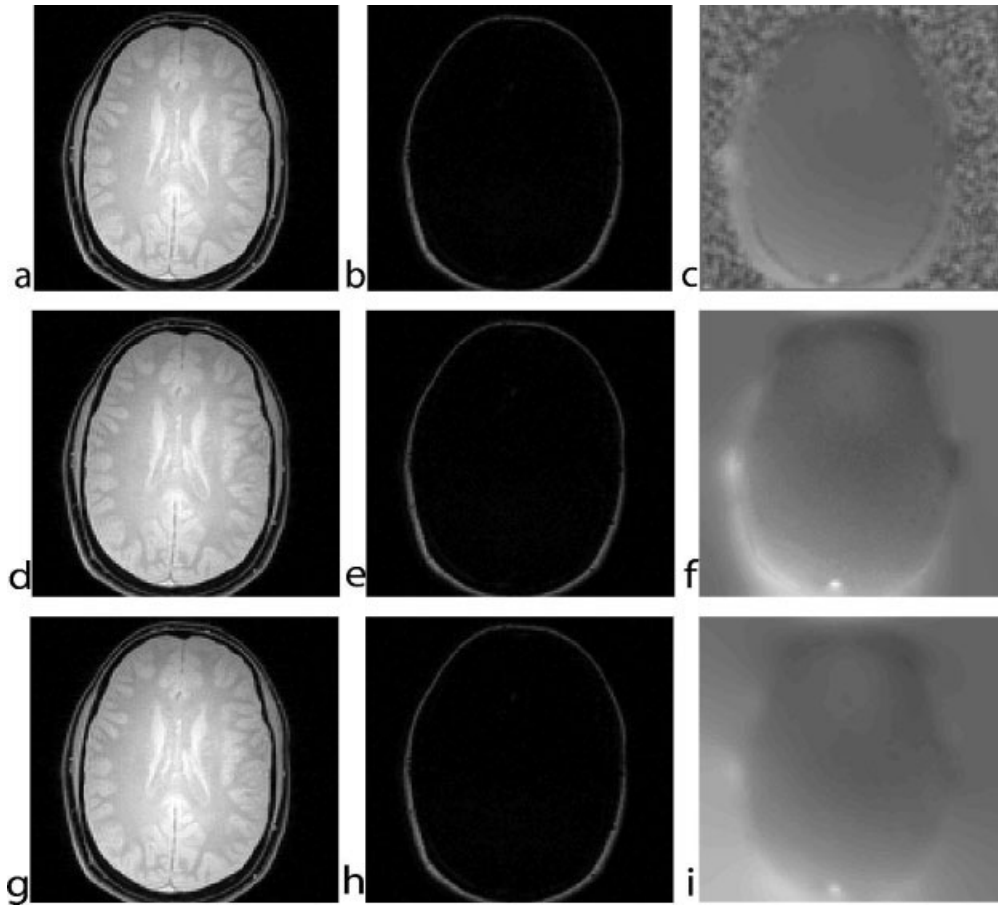


FIG. 3. Water/fat decomposition from a brain acquisition. The first column contains the estimated water component using the different algorithms. The second column contains the estimated fat component. The third column contains the regularized field map. (a–c) IDEAL estimates. The smooth field map is obtained by filtering the raw field map (resulting from voxel-by-voxel estimation) with a smoothing kernel (3); (d–f) VARPRO estimates. The smooth field map is obtained directly by applying an MRF prior; (g–i) LP estimates. The smooth field map is obtained by weighted LS regularization of the raw field map.

map estimates are proportional to the amplitudes of the corresponding components.

To test the multicoil version of the proposed methods, a multicoil acquisition of the abdomen was performed using six different TE values, {1.5, 2.0, 3.6, 5.1, 6.6, 8.2} ms, corresponding to relative water/fat phases  $\{-7\pi/5, -7\pi/6, -\pi/2, \pi/6, 5\pi/6, 3\pi/2\}$ . Data were collected on a GE 1.5 Tesla whole body scanner (GE Healthcare Technologies, Waukesha, WI) using a four-channel torso phased-array receiver coil. The pulse sequence used was a 3D fast spoiled gradient echo sequence. Each 3D data set (for a corresponding echo time) was acquired in a single but separate breath hold. All data were collected in accordance with the local institutional review board.

The multicoil results are shown in Fig. 4. Figures 4a–c show the “gold standard” decomposition obtained from VARPRO using all six shifts. Figures 4d–f show the results from VARPRO using only three different echo times (with water/fat phases  $\{-7\pi/6, -\pi/2, \pi/6\}$ ). Figures 4g–i show the resulting decomposition from the same three echo times, using the LP method. Note the high quality of the decompositions obtained with both methods using just three echo times.

Figure 5 shows a comparison of IDEAL and the proposed VARPRO method in the presence of high field inhomogeneity. The images were acquired with water/fat phases  $\{7\pi/6, \pi/2, -\pi/6\}$ , on a 3 T Siemens Allegra head scanner in accordance with the local institutional review board. The field inhomogeneity reached approximately 360 Hz. The VARPRO method included spatial regularization using ICM. Note how IDEAL swaps the different components in part of the image, whereas the proposed method is able to correctly separate the water and fat signals. This increased robustness is due to the global optimality of the VARPRO approach, regardless of the nonconvexity of  $R(f_B)$ , and the improved method for imposing spatial smoothness on the field map (which is performed jointly with the water/fat estimation, instead of in a separate step). A region-growing method (10) is also expected to perform well for this type of dataset. However, the fact that VARPRO produces good results in this case (using the same parameters as in the moderate field inhomogeneity cases) highlights the robustness of the proposed method. Although ICM only guarantees convergence to a local optimum of the a posteriori distribution, ICM-based field map estimation is less dependent (compared to region-growing)

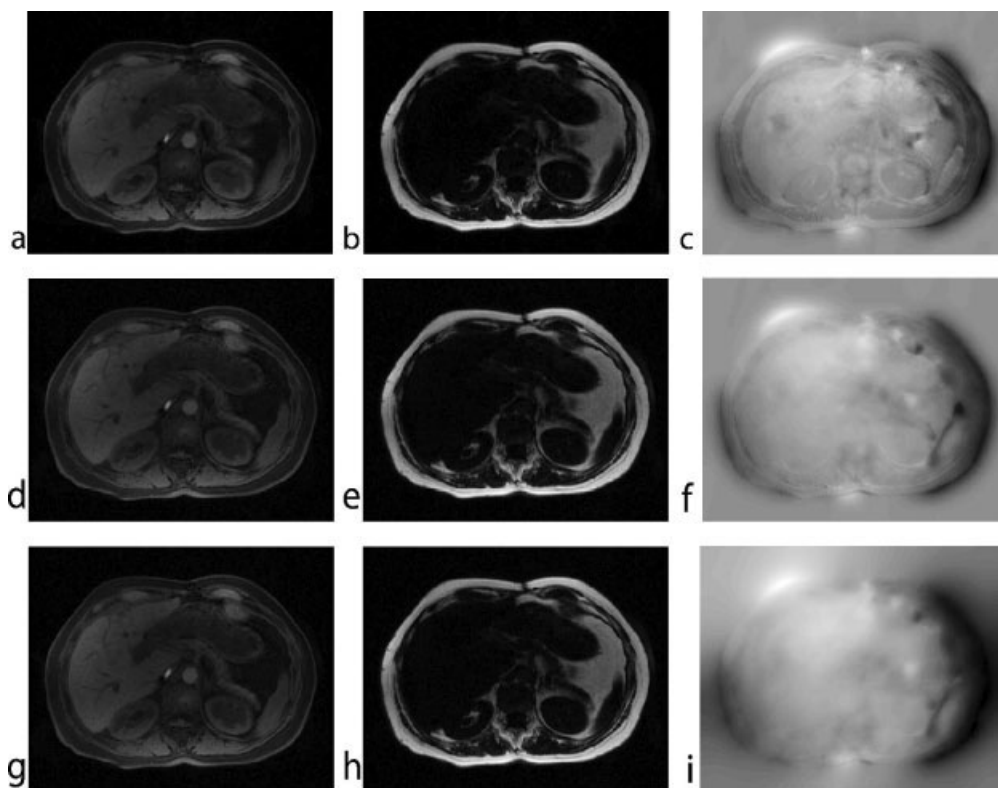


FIG. 4. Water/fat decomposition from a multicoil abdominal acquisition. The first column contains the estimated water component using the different algorithms. The second column contains the estimated fat component. Both components are displayed using sum of squares combination of the multicoil signal. The third column contains the regularized field map. (a–c) VARPRO estimates using all six echo time shifts; (d–f) VARPRO estimates using three water/fat shifts; (g–i) LP estimates using three water/fat shifts.

on the initial values assigned to the field map (which is set to all zeros at the beginning of the ICM iteration for all the results presented in this paper).

The three methods considered in this article present different computational requirements. In IDEAL, most of the computation time is spent solving two small systems of linear equations for updating the estimated field value and the water/fat amplitudes (3). This is done iteratively (until a convergence criterion is satisfied) for each voxel from each coil. While an iterative procedure may potentially require many iterations to converge, in our experience convergence typically occurs in a few iterations, so the method is quite fast. After the voxel-by-voxel iterative procedure, low-pass filtering the field map estimate and recomputing the water/fat images is done very rapidly. In VARPRO, first the residual (Eq. [6]) must be computed for all voxels and field map values, and next the field map is estimated by repeatedly updating its value at all voxels according to Eq. [10]. Subsequent estimation of the water/fat images given the field map requires negligible computation. In LP, the main computational burden consists of solving a small linear system and polynomial rooting at each voxel with signal above the noise threshold, and smoothing the estimated field map by solving a regularized LS problem. We compared our own Matlab (The Mathworks, Natick, MA) implementations

of IDEAL, VARPRO, and LP. Note that the execution times reported here are expected to decrease dramatically when optimized and coded in C on a fast, multiprocessor architecture. For a single-coil, three-point dataset with images of size  $128 \times 128$ , the voxel-by-voxel IDEAL method followed by low-pass filtering of the fieldmap and reestimation of the water/fat amplitudes throughout the image (as described in (3)) required 16.5 sec on an Intel Xeon-based desktop PC at 3.6 GHz with 8 GB of RAM. To solve the same problem, the VARPRO method with MRF prior, with  $L = 300$  field inhomogeneity values and 30 ICM iterations required 64.3 sec, whereas the LP method using weighted LS field map regularization required 18.8 sec.

Multicoil acquisitions (number of channels  $P > 1$ ) are handled by the proposed methods with a small increase in computation time. For an eight-coil ( $P = 8$ ), three-point dataset with images of size  $128 \times 128$ , the computation time for IDEAL was 114.4 sec, while VARPRO required 79.8 sec and LP required 39.4 sec. The observed differences are mainly due to the fact that the proposed methods directly impose the presence of a unique field map (thus solving the same nonlinear problem as in the single-coil case), whereas IDEAL solves  $P$  nonlinear problems and then combines the resulting field maps. This does not imply any fundamental limitation of IDEAL: the proposed multicoil formulation

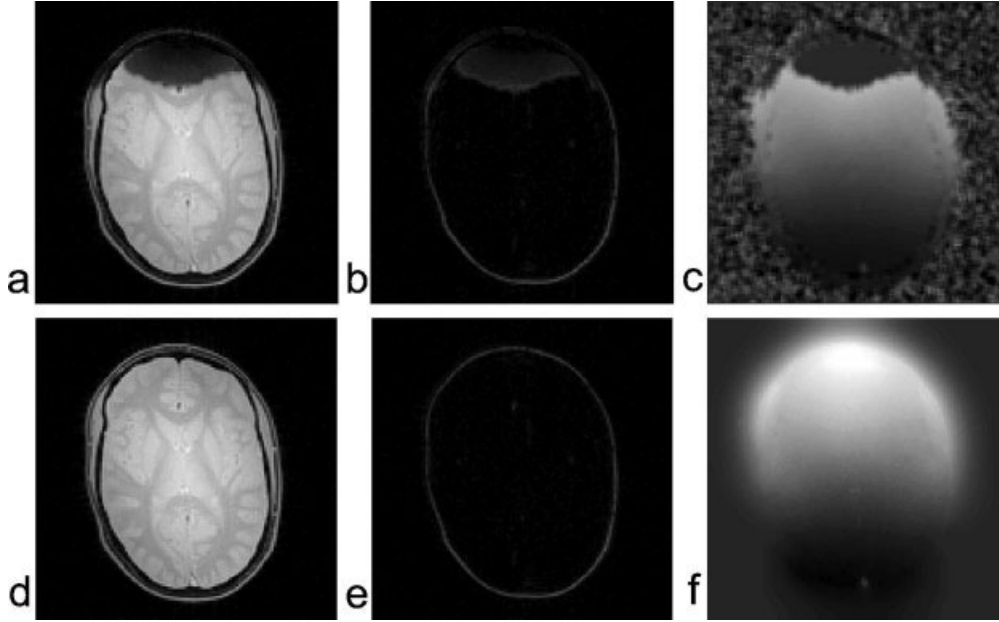


FIG. 5. Comparison of IDEAL and VARPRO results in the presence of high field inhomogeneity. (a–c) IDEAL estimates for water, fat, and field map, respectively; (d–f) VARPRO estimates for water, fat, and field map, respectively.

used with VARPRO in this paper can be incorporated into the IDEAL algorithm.

In recent work, Yu et al. proposed an extension of the IDEAL algorithm to include simultaneous estimation of  $T_2^*$  (24). Relaxation effects are naturally accounted for within the LP formulation. However, to take relaxation effects into account,  $|z_n| < 1$  in Eq. [14], and thus forward and backward linear prediction cannot be used simultaneously as in the  $|z_n| = 1$  case. For example, if two damped components are to be estimated, at least four uniformly spaced data points need to be acquired. Clearly, the VARPRO method can be applied for the estimation of multiple nonlinear parameters (e.g., relaxation effects). However, the computational demands increase significantly with the number of nonlinear parameters.

Both VARPRO and LP can be used to estimate multiple chemical species. If the chemical shifts are known exactly, then VARPRO is very efficient and robust (since the problem still reduces to a one-dimensional search). On the other hand, LP estimates all the chemical shifts and thus requires a larger number of measurements. Both methods have been studied extensively in the context of MR spectroscopy quantitation (25).

## CONCLUSIONS

This article presented two novel methods for joint estimation of water/fat images and field inhomogeneity map from Dixon-type acquisitions. The VARPRO method overcomes several limitations of previously proposed descent-based algorithms. First, it provides an efficient and globally optimal solution to the nonconvex NLLS problem. Second, spatial smoothness constraints on the field map estimate are enforced in a statistically meaningful way using an MRF prior. The LP method produces good results under

moderate noise and field inhomogeneity conditions and is computationally very efficient. This method can be used as long as the echo times are uniformly spaced. Both LP and VARPRO allow natural extensions to handle multicoil acquisitions, as well as cases in which there are more than two chemical species, or when relaxation effects cannot be neglected.

## APPENDIX

One key aspect of the proposed VARPRO method is the discretization of the feasible range of main field values as a finite set of values  $\{f_{B,l}\}_{l=1}^L$ . An important requirement for the minimizing solution to be meaningful is that the spacing is small enough relative to the variability of  $R(f_B)$ . In other words, we need to guarantee that  $R(f_B)$  does not contain abrupt changes which are not captured by the discretized version  $\{R(f_{B,l})\}_{l=1}^L$ . For this purpose, let us consider the derivative of  $R(f_B)$ . From Eq. [6],

$$\frac{dR(f_B)}{df_B} = - \sum_{\substack{m,n \\ m \neq n}} s^*(t_n) s(t_m) \Gamma_{n,m} e^{i2\pi f_B(t_n - t_m)} 2\pi(t_n - t_m)$$

where  $\Gamma = \Phi(\Phi^H \Phi)^{-1} \Phi^H$ . The following bound follows readily:

$$\left| \frac{dR(f_B)}{df_B} \right| \leq |\max_k s(t_k)|^2 \sum_{\substack{m,n \\ m \neq n}} |\Gamma_{n,m} 2\pi(t_n - t_m)| = B. \quad [A1]$$

Given the discretization spacing  $\Delta f_B = f_{B,l+1} - f_{B,l}$ , this provides a bound on the maximum difference of the global

optimum of the continuous function  $R(f_B)$  from the discretized version  $\{R(f_{B,l})\}_{l=1}^T$ :

$$\left| \min_{f_B \in [f_{B,\text{MIN}}, f_{B,\text{MAX}}]} R(f_B) - \min_{l=1,2,\dots,L} \{R(f_{B,l})\}_{l=1}^L \right| \leq \frac{\Delta f_B}{2} B \quad [\text{A2}]$$

which produces a useful criterion to ensure that the cost function  $R(f_B)$  is smooth with respect to  $\Delta f_B$ . For example, let us consider the signal from voxel (65, 65) in the brain acquisition shown in Fig. 3. Using field inhomogeneity bounds  $\pm 400$  Hz with  $L = 300$  uniformly spaced discretized values, Eq. [A2] guarantees that the difference between the minimal residual in the discretized and continuous problems will be at most 0.6% of the range of the residual.

## LIST OF SYMBOLS

$a_m$	LP amplitude corresponding to $m$ th component
$B_0$	main (static) magnetic field (T)
$\mathbf{D}$	matrix for computing 2D finite-differences for regularization of field map
$f_B$	off-resonance frequency caused by field inhomogeneity (Hz)
$f_{B,v}$	single-voxel LP estimate of field inhomogeneity (Hz)
$f_B^o$	optimal estimate for field inhomogeneity (Hz)
$f_{B,\text{MIN}}$	lower bound on the field inhomogeneity (Hz)
$f_{B,\text{MAX}}$	upper bound on the field inhomogeneity (Hz)
$f_B^q$	field inhomogeneity at voxel $q$ (Hz)
$f_B^{q,\text{cur}}$	current value of field inhomogeneity at voxel $q$ (Hz)
$f_B^{q,\text{new}}$	updated value of field inhomogeneity at voxel $q$ (Hz)
$f_F$	chemical shift between water and fat (Hz)
$\mathbf{f}_B$	vector containing the complete field map (Hz)
$\mathbf{f}_{B,v}$	vector containing the field map estimated voxel-by voxel (Hz)
$\hat{\mathbf{f}}_B$	regularized field map (Hz)
$g_m$	$m$ th LP coefficient
$\mathbf{g}$	LP coefficient vector
$G$	polynomial associated with LP coefficient vector
$\mathbf{I}$	identity matrix
$L$	number of different field inhomogeneity values for discretization in VARPRO
$N$	number of acquisitions
$P$	number of distinct coils in multicoil acquisitions
$Q$	number of voxels in image
$R$	maximum-likelihood cost function in the VARPRO formulation
$R_0$	original maximum-likelihood cost function
$R_{p,0}$	original maximum-likelihood cost function for signal from $p$ th coil
$R_{\text{MC}}$	augmented cost function for multicoil acquisitions (VARPRO formulation)
$R_{\text{MC},0}$	augmented cost function for multicoil acquisitions acquired signal at a given echo time
$s$	acquired signal from a given echo time
$s_p$	acquired signal from coil $p$ at a given echo time
$\mathbf{s}$	vector of acquired signals at different times
$t_n$	echo time of the $n$ th acquisition (sec)
$\mathbf{W}$	weighting matrix for field map regularization in LP method

$z_m$	LP pole corresponding to $m$ th component
$\mathbf{\Gamma}$	matrix used in the derivation of the bound on the accuracy of the VARPRO discretization
$\delta q$	neighborhood of voxel $q$ in MRF formulation
$\Delta t$	spacing between echo times of consecutive acquisitions (sec)
$\varepsilon$	threshold for stopping criterion in ICM iteration
$\lambda$	regularization parameter for LP method
$\mathbf{\Lambda}$	diagonal matrix applying effect of field inhomogeneity into signal
$\mu$	regularization parameter for VARPRO method with MRF prior
$\rho_W$	amplitude of water component
$\rho_F$	amplitude of fat component
$\rho_{W,p}$	amplitude of water component in $p$ th image (multicoil acquisitions)
$\rho_{F,p}$	amplitude of fat component in $p$ th image (multicoil acquisitions)
$\boldsymbol{\rho}$	vector containing both water and fat amplitudes
$\boldsymbol{\rho}_p$	vector containing both water and fat amplitudes in $p$ th image (multicoil acquisitions)
$\boldsymbol{\rho}^o$	optimal estimate for water and fat amplitudes
$\phi_m$	estimated frequency of $m$ th component detected with LP (Hz)
$\phi_F$	estimated frequency of component assigned to fat (Hz)
$\phi_W$	estimated frequency of component assigned to water (Hz)
$\Phi$	matrix mapping amplitudes into signal samples in the absence of field inhomogeneity
$\Psi$	matrix mapping component amplitudes to signal samples

## REFERENCES

- Dixon WT. Simple proton spectroscopic imaging. *Radiology* 1984;153:189–194.
- Glover GH, Schneider E. Three-point Dixon technique for true water/fat decomposition with  $B_0$  inhomogeneity correction. *Magn Reson Med* 1991;18:371–383.
- Reeder SB, Wen Z, Yu H, Pineda AR, Gold GE, Markl M, Pelc NJ. Multicoil Dixon chemical species separation with an iterative least squares estimation method. *Magn Reson Med* 2004;51:35–45.
- Reeder SB, Pineda AR, Wen Z, Shimakawa A, Yu H, Brittain JH, Gold GE, Beaulieu CH, Pelc NJ. Iterative decomposition of water and fat with echo asymmetry and least-squares estimation (IDEAL): Application with fast spin-echo imaging. *Magn Reson Med* 2005;54:636–644.
- Bernstein MA, King KF, Zhou XJ. *Handbook of MRI pulse sequences*. Burlington, MA: Elsevier Academic Press; 2004.
- Pineda A, Reeder S, Wen Z, Pelc NJ. Cramér-Rao bounds for three-point decomposition of water and fat. *Magn Reson Med* 2005;54:625–635.
- Golub G, Pereyra V. Separable nonlinear least squares: The variable projection method and its applications. *Inverse Prob* 2003;19:R1–R26.
- Boada F, Liang ZP, Haacke EM. Improved parametric reconstruction using variable projection optimization. *Inverse Probab* 1998;14:19–27.
- Haldar JP, Anderson J, Sun SW. Maximum likelihood estimation of  $T_1$  relaxation parameters using VARPRO. In *Proceedings of the 15th Annual Meeting of ISMRM, Berlin, Germany, 2007 (Abstract 41)*.
- Yu H, Reeder SB, Shimakawa A, Brittain JH, Pelc NJ. Field map estimation with a region growing scheme for iterative 3-point water-fat decomposition. *Magn Reson Med* 2005;54:1032–1039.
- Bhagwandien R, Moerland MA, Bakker CJG, Beersma R, Lagendijk JJW. Numerical analysis of the magnetic field for arbitrary magnetic susceptibility distributions in 3D. *Magn Reson Imaging* 1994;12:101–107.

12. Schomberg H. Off-resonance correction of MR images. *IEEE Trans Med Imaging* 1999;18:481–495.
13. Fessler JA, Yao D, Noll DC. Regularized fieldmap estimation in MRI. In *Proceedings of the 3rd IEEE International Symposium on Biomedical Imaging: Macro to Nano*, Arlington, VA, USA, 2006, pp 706–709.
14. Geman S, Geman D. Stochastic relaxation, Gibbs distribution and the Bayesian restoration of images. *IEEE Trans Pattern Anal Mach Intell* 1984;6:712–741.
15. Besag J. On the statistical analysis of dirty pictures. *J R Stat Soc Ser B* 1986;48:259–302.
16. Kellman P, McVeigh ER. Image reconstruction in SNR units: a general method for SNR measurement. *Magn Reson Med* 2005;54:1439–1447.
17. Roemer PB, Eldelstein WA, Souza SP, Hayes CE, Mueller OM. The NMR phased array. *Magn Reson Med* 1990;16:192–225.
18. Hayes CE, Roemer PB. Noise correlations in data simultaneously acquired from multiple surface coil arrays. *Magn Reson Med* 1990;16:181–191.
19. Bernstein MA, Grgic M, Brosnan TJ, Pelc NJ. Reconstructions of phase contrast, phased array multicoil data. *Magn Reson Med* 1994;32:330–334.
20. Kumaresan R. On the zeros of the linear prediction-error filter for deterministic signals. *IEEE Trans Acoust* 1983;31:217–220.
21. Ulrych TJ, Clayton RW. Time series modelling and maximum entropy. *Phys Earth Planet Int* 1976;12:188–200.
22. Vogel CR. *Computational methods for inverse problems*. Philadelphia, PA, USA: SIAM; 2002.
23. van Trees HL. *Detection, estimation and modulation theory, part I*. New York: Wiley; 1968.
24. Yu H, McKenzie A, Shimakawa A, Pelc NJ, Brittain JH, Reeder SB. IDEAL water-fat separation with simultaneous  $T_2^*$  estimation. In *Proceedings of the 14th Annual Meeting of ISMRM*, Seattle, WA, USA, 2006 (Abstract 624).
25. Vanhamme L, Sundin T, van Hecke P, van Huffel S. MR spectroscopy quantitation: A review of time-domain methods. *NMR Biomed* 2001;14:233–246.